ISSN 1990-3413, Astrophysical Bulletin, 2015, Vol. 70, No. 3, pp. 243–256. © Pleiades Publishing, Ltd., 2015.
Original Russian Text © A.I. Kopylov, F.G. Kopylova, 2015, published in Astrofizicheskii Byulleten, 2015, Vol. 70, No. 3, pp. 257–270.

Structure of Galaxy Groups and Clusters and Measurement of Their Masses

A. I. Kopylov* **and F. G. Kopylova****

Special Astrophysical Observatory, Russian Academy of Sciences, Nizhnii Arkhyz, 369167 Russia

Received April 8, 2015; in final form, June 9, 2015

Abstract—We report the results of measurement and comparison of masses for a sample of 29 groups and clusters of galaxies ($z < 0.1$). We use the SDSS DR7 archive data to determine dynamical masses from the one-dimensional dispersion of line-of-sight velocities for virialized regions of radii R_{200} and R_e. Our method for determination of effective radii of galaxy systems from the cumulative distribution of the number of galaxies depending on squared clustercentric distance allowed us to estimate masses $M_{1/2}$ (within R_e), which are related to the masses contained inside R_{200}: $M_{200} \sim 1.65\,M_{1/2}$. A comparison of the inferred dynamic masses and the hydrostatic masses determined from the radiation of hot gas in galaxy groups and clusters (based on published data) led us to conclude that the inferred masses for the main sample of 21 groups and clusters agree to within 12%. These systems also obey the relation $M_{X,200} \sim 1.65\,M_{1/2}$. For the remaining eight systems, which are mostly located in the Hercules supercluster, the discrepancy between the hydrostatic and the dynamic masses amounts to 2σ. This discrepancy is most likely due to the incompleteness of the formation processes of these clusters via hierarchical merger in the region of the rich Hercules supercluster.

DOI: 10.1134/S1990341315030013

Keywords: *galaxies: clusters: general—galaxies: groups: general*

1. INTRODUCTION

Galaxy clusters are the largest gravitationally bound structures in the Universe. About 80–90% of their mass is in the form of dark matter, and the remaining mass is represented by baryons, most of which (10–20%) are in the form of hot diffuse plasma with $T > 10^7$ K (it is the main component of the inner medium of galaxy clusters), which emits mostly in the x-ray domain. Galaxies contribute only several percent of the cluster mass. The mass function of galaxy clusters is sensitive to cosmological parameters, turning the measurement of their accurate masses a challenging task [1]. Several methods have been developed for measuring the masses of galaxy clusters with different degree of accuracy. Dynamical methods use the dispersion of line-of-sight velocities of galaxies: masses of galaxy systems can be determined from the condition of virial equilibrium (e.g., [2–4]). Another method uses the data for the x-ray emission from hot gas in clusters to determine the masses of galaxy systems under the assumptions of spherical symmetry and hydrostatic equilibrium (e.g., [5–7]). The masses of clusters can be determined without extra assumptions from gravitational lensing of background galaxies (e.g., [8]), however, the inferred masses depend on the orientation of the systems studied with respect to the line of sight. The method of caustics, which is based on the analysis of the distribution of galaxy redshifts and escape velocity from the cluster [9], also requires no additional assumptions. The total mass of galaxy groups and clusters within the radius R_0 that separates them from global cosmic expansion is measured assuming that the cluster is spherically symmetric and that tangential velocities of galaxies at its periphery are negligible [10].

The aim of this study is to measure the dynamical masses of 29 groups and clusters of galaxies using various methods, intercompare the resulting mass estimates, and compare them with the masses inferred from the x-ray emission of gas. The entire sample studied consists of 148 groups and clusters of galaxies selected from large superclusters, double systems, and field objects in the redshift interval $0.02 < z < 0.1$. In this paper we report the results for clusters with available mass estimates from (published) hot gas x-ray emission data. We made use of the data from the SDSS (Sloan Digital Sky Survey)

*E-mail: akop@sao.ru
**E-mail: flera@sao.ru

Table 1. Physical properties of galaxy groups and clusters within R_{200}

Cluster	$z_{\rm h}$	N_z	R_{200}, Mpc	$\sigma_{\rm c}$, km s^{-1}	M_{200}, $10^{14}\,M_\odot$	$L_{K,200}$, $10^{12}\,L_\odot$	$M_{X,200}$, $10^{14}\,M_\odot$	$L_{K,X200}$, $10^{12}\,L_\odot$	References
Virgo	0.003821	132	1.63	661	4.99 ± 1.31	6.12	1.46	3.26	[5]
A 1656	0.023282	681	2.26	924	13.52 ± 1.49	16.69	11.90 ± 1.95	16.72	[7, 17]
MKW 08	0.026906	103	1.10	450	1.56 ± 0.46	3.16	1.91 ± 0.30	3.31	[7, 17, 18]
UGC 05088	0.027622	13	0.60	247	0.26 ± 0.22	0.52	0.22 ± 0.08	0.53	[19]
NGC 6338	0.029342	83	1.35	552	2.87 ± 0.94	2.82	0.92 ± 0.12	2.25	[5, 18, 19]
A 2199	0.030458	288	1.82	746	7.09 ± 1.25	10.13	3.78 ± 0.59	9.04	[5, 7, 17, 20]
AWM 4	0.031827	37	0.93	380	0.94 ± 0.46	1.53	1.67	1.56	[20]
A 1177	0.032159	26	0.82	337	0.65 ± 0.35	1.23	0.86 ± 0.12	1.35	[18, 19]
A 2063	0.034664	146	1.83	753	7.28 ± 1.80	6.12	3.27 ± 0.32	5.51	[5, 7, 17, 20]
A 2052	0.034726	116	1.52	623	4.12 ± 1.15	4.96	2.89 ± 0.28	4.80	[5, 7, 17, 20, 21]
AWM 5	0.035043	52	1.29	528	2.51 ± 1.04	4.02	0.98 ± 0.24	3.52	[18, 19]
A 2147	0.036179	344	2.08	853	10.57 ± 1.71	13.00	2.88 ± 0.58	9.84	[7, 17]
A 2151	0.036378	255	1.78	734	6.74 ± 1.27	12.15	1.66 ± 0.07	8.00	[7, 17]
NGC 5098	0.036812	58	1.08	445	1.50 ± 0.59	2.88	0.25 ± 0.03	1.97	[19, 22]
A 1139	0.039327	80	1.12	459	1.64 ± 0.55	3.68	1.24	3.40	[19]
A 1983	0.044803	97	1.12	460	1.65 ± 0.51	4.98	1.59	4.96	[23]
MKW 03s	0.044953	82	1.47	608	3.81 ± 1.26	4.68	2.79 ± 0.25	4.25	[5, 7, 17, 20, 21]
RXCJ 1022	0.054163	59	1.33	551	2.83 ± 1.11	4.43	0.98 ± 0.16	3.25	[18, 19]
A 1991	0.058463	79	1.33	554	2.87 ± 0.96	6.40	1.77 ± 0.08	5.19	[6, 19, 23]
A 1795	0.062444	123	1.86	775	7.83 ± 2.12	9.00	9.60 ± 0.65	9.05	[5–7, 17, 20, 21]
A 1275	0.062750	22	0.84	348	0.71 ± 0.51	1.93	0.94	1.98	[19]
A 2092	0.066564	37	1.17	486	1.93 ± 0.88	3.28	1.29	3.06	[19]
A 2065	0.072211	210	2.64	1104	22.53 ± 4.29	20.31	13.94 ± 2.75	18.11	[7, 17]
A 0744	0.072812	19	1.05	440	1.43 ± 0.98	2.89	1.43	2.25	[19]
A 1238	0.074111	61	1.29	541	2.65 ± 1.01	6.01	1.72	5.48	[19]
A 1775B	0.075138	62	1.39	581	3.28 ± 1.25	6.00	4.20 ± 0.02	6.61	[7, 17]
A 1800	0.075321	67	1.68	705	5.86 ± 2.14	8.22	5.82 ± 0.13	8.22	[7, 17]
A 2029	0.078145	180	2.50	1046	19.11 ± 4.28	23.58	12.17 ± 0.65	18.76	[5–7, 17, 20]
A 2142	0.090135	191	2.28	963	14.82 ± 3.23	26.48	13.92 ± 0.79	26.44	[5, 7, 17]

and 2MASS XSC (Two Micron All Sky Survey Extended Source Catalog).

The paper has the following layout. Section 2 describes the measurements of the dynamical masses of galaxy clusters: the M_{200} masses contained inside the R_{200} radius and the $M_{1/2}$ masses contained inside the effective radius R_e. Section 3 describes the measurements of the $M_{X,200}$ masses of galaxy clusters based on their hot gas emission. In Section 4 we analyze our results. The conclusions section summarizes the main results. Here we use the following values of cosmological parameters: $\Omega_m = 0.3$, $\Omega_\Lambda = 0.7$, $H_0 = 70\ \mathrm{km\,s^{-1}\,Mpc^{-1}}$.

2. METHODS FOR MEASUREMENT OF MASSES OF GALAXY GROUPS AND CLUSTERS

2.1. Measurement of the M_{200} Mass

Objects in our sample of 29 groups and clusters of galaxies have redshifts in the interval $0.003 < z < 0.1$. Galaxy systems are usually subdivided into groups and clusters in accordance with their masses or line-of-sight velocity dispersions σ of individual galaxies. For example, Nurmi et al. [11] used SDSS data to find that line-of-sight velocity dispersions of galaxy groups with $N_{\mathrm{gal}} \geq 10$ members do not exceed 400 $\mathrm{km\,s^{-1}}$, i.e., their masses do not exceed $10^{14}\ M_\odot$. Several galaxy systems in our sample—A 1177, A 1275, AWM 4, UGC 05088—have parameters typical of groups. For galaxies we used the spectroscopic data from the SDSS catalog (Data Release 7, [12]) supplemented with the data from NASA Extragalactic Database (NED). We determined the dynamical masses of clusters from the dispersions of line-of-sight velocities of galaxies assuming that the systems are in virial equilibrium. Carlberg et al. [13] determined the empirical radius R_{200} from the virial radius ($R_{200} < R_{\mathrm{vir}}$), which can be inferred from the dispersion of line-of-sight velocities of galaxies provided that $M(r) \propto r$. Density inside this radius exceeds 200 times the critical density of the Universe. This radius can be estimated by the formula $R_{200} = \sqrt{3}\sigma/(10H(z))$ Mpc. Hence if the cluster can be considered to be virialized inside this radius, its mass M_{200} can be computed by the formula $M_{200} = 3G^{-1}R_{200}\sigma^2$, where σ is the dispersion of line-of-sight velocities of galaxies located inside the R_{200} radius, and G is the gravitational constant. Hence $M_{200} \propto \sigma^3$. The inferred mass is less than the total mass M_{vir}, because clusters are virialized even at $R_{100} \sim 1.3\,R_{200}$ (e.g., [14]). We thus first estimate the average line-of-sight velocity cz of the cluster and its dispersion σ, and then use the inferred dispersion to determine the R_{200} radius. We then determine the number of galaxies within this radius and redetermine cz, σ, and R_{200}, etc. We move from the cluster center and determine iteratively the dispersion of line-of-sight velocities of galaxies and other parameters of clusters within this radius. We consider galaxies with velocities deviating by more than 2.7σ from the mean velocity of the group (see, e.g., [15]) as field objects. Selection criteria usually vary from 2.5σ to 3.0σ.

According to numerical simulations [16], the computed virial masses of galaxy clusters within certain radii (e.g., the harmonic radius) should be corrected to account for the fact that some members of the systems are located beyond this radius. At the same time, the technique that we use to determine the mass from the dispersion of line-of-sight velocities of galaxies requires no such correction. The computed dispersion of line-of-sight velocities of galaxies can be both underestimated and overestimated depending on the presence of galaxy groups along the line of sight toward the cluster studied.

To characterize the structure and kinematics of each cluster and its nearest neighborhood in more detail, we show in Figs. 1 and 2 (by way of example) the following diagrams for galaxies of Virgo and NGC 5098 clusters.

(1) Scatter of line-of-sight velocities of cluster members and galaxies considered to be field objects as a function of squared clustercentric distance.

(2) Cumulative distribution of the number of galaxies as a function of the squared radius in order to visualize the identification of the dense core of the cluster, its more tenuous halo, and the external region where the distribution becomes linear in the adopted coordinates, i.e., where the distribution of surrounding galaxies becomes uniform on the average.

(3) Location of galaxies in the sky plane in equatorial coordinates.

(4) Histogram of line-of-sight velocities of all galaxies within the R_{200} radius (the solid lines shows the Gaussian corresponding to the dispersion of line-of-sight velocities of clusters from Table 1). The dashed line shows the Gaussian corresponding only to the galaxies located within the selected peak in the histogram. We discuss them in more detail in the next subsection. We selected early-type galaxies based on the following parameters that characterize their SDSS r-band images: fracDeV ≥ 0.8, where fracDeV is the bulge contribution to the surface brightness profile of the galaxy; $r_{90}/r_{50} \geq 2.6$, where $c = r_{90}/r_{50}$ is the concentration index equal to the ratio of the radii containing 90% and 50% ofthe

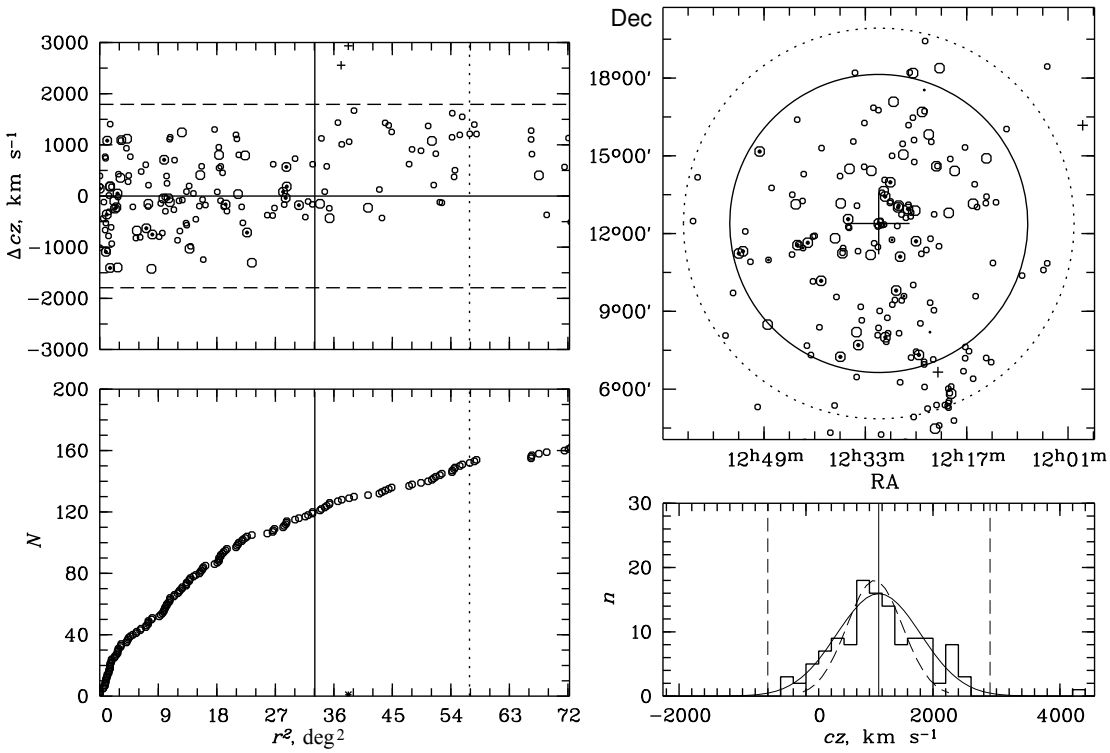

Fig. 1. Distribution of galaxies in the Virgo cluster ($M_K < -21^{\rm m}$). The top left panel shows the deviations of line-of-sight velocities of galaxies from the mean line-of-sight velocity of the cluster, determined from objects located within R_{200}. The horizontal dashed lines indicate the $\pm 2.7\sigma$ deviations, the solid vertical line indicates the R_{200} radius, and the dotted line is the Abell radius (2.14 Mpc). Large circles represent galaxies brighter than $M_K^* + 1 = -23\overset{\rm m}{.}97$; circles with a dot inside—early-type galaxies; pluses and crosses—the background and foreground galaxies respectively. The bottom left panel shows the cumulative distribution of the number of galaxies as a function of squared clustercentric distance. The circles correspond to galaxies shown as circles in the top left figure, and asterisks denote field objects. The top right panel shows the same galaxies as in the top left panel (same designations used) but in equatorial coordinates. The circles show the R_{200} radius (the solid line) and the Abell radius (the dotted line). The large cross indicates the position of the cluster center. The bottom right panel shows the distribution of line-of-sight velocities of all galaxies located within R_{200} (the solid line shows the Gaussian for cluster members corresponding to σ of the cluster). The dashed line shows the Gaussian corresponding to σ computed from $M_{X,200}$. The solid vertical line shows the mean line-of-sight velocity of the cluster, and the dashed lines correspond to the $\pm 2.7\sigma$ deviations.

Petrosian flux, respectively. We also imposed the additional color cut $\Delta(u-r) > -0.2$. In the figures the corresponding galaxies are marked by the dot inside the circle.

We reported our measured M_{200} masses of galaxy groups and clusters in the regions of Ursa Major, Leo, and Hercules superclusters and four bimodal clusters with the largest differences of line-of-sight velocities (about 3000 km s^{-1}) in our previous papers [24–30]. Both in the above papers and in this study we also determined the infrared (IR) luminosities of the galaxy systems for galaxies with $M_K < -21^{\rm m}$ (the magnitudes are in the $K_{\rm s}$-band filter of the 2MASS extended source catalog).

Table 1 lists the results of our measurements of the properties of the galaxy clusters in the region of radius R_{200} studied in this paper: cluster name; heliocentric redshift; number of galaxies with measuredredshifts ($r_{\rm pet} < 17\overset{\rm m}{.}77$); the R_{200} radius in Mpc; $\sigma_{\rm c}$, the dispersion of line-of-sight velocities with cosmological correction $(1+z)^{-1}$ applied; the M_{200} mass; IR luminosity $L_{K,200}$ ($M_K < -21^{\rm m}$); the $M_{X,200}$ mass determined from the x-ray emission of the cluster gas (usually converted from $M_{X,500}$); the IR luminosity $L_{K,X200}$ ($M_K < -21^{\rm m}$) computed for the $M_{X,200}$ mass using the above formulas. The last column of the table gives the references to the sources of the $M_{X,200}$ mass estimates used. The errors of the measured M_{200} and L_K are computed by propagating the errors of measured $\sigma_{\rm c}$ (hereafter referred to as σ). Note that the errors of the measured L_K are small and insignificant. In the cases where only one $M_{X,200}$ measurement is available no errors are listed in the table, whereas in all the remaining cases the listed measurement errors for $M_{X,200}$ are the errors of the mean.

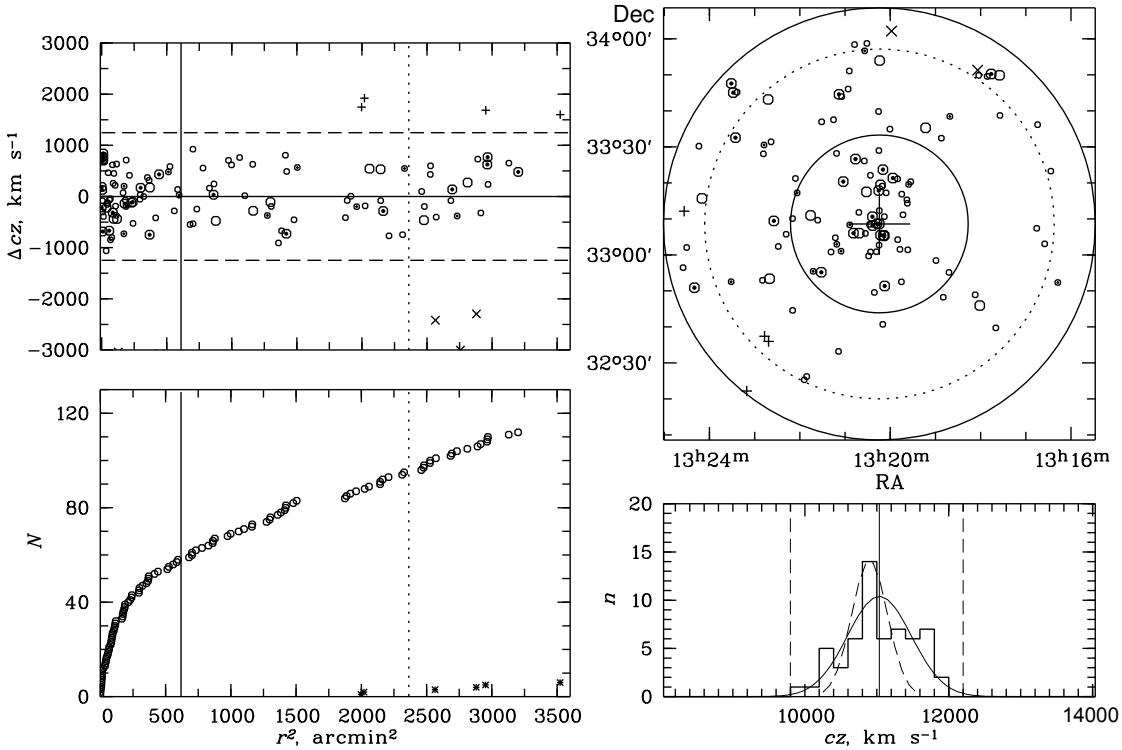

Fig. 2. Distribution of galaxies in NGC 5098. The structure and designations in Figs. 1 and 2 are the same. The region studied is limited by a circle with a radius of 95′ (the solid line).

2.2. Measurement of the $M_{1/2}$ Mass

Tollerud et al. [31] show that the masses of spheroidal galaxies (including the brightest galaxies in the clusters) with measured dispersions of line-of-sight velocities can be determined for the characteristic radius, which is approximately equal to the 3D radius of the galaxy containing half of its luminosity. As a result, the virial mass of the galaxy is measured, which is independent of the anisotropy of stellar velocities [32] and which is equal to $M_{1/2} = 3G^{-1}\,\sigma^2_{1/2}\,r_{1/2}$, where $r_{1/2} = 4/3R_{\rm e}$ ($R_{\rm e}$ is the effective radius containing half of the luminosity emitted by the galaxy); G is the gravitational constant, and σ, the dispersion of line-of-sight velocities of stars in the galaxy. Given that galaxy clusters, like spheroidal galaxies, obey the "fundamental plane" determined by the dispersion of line-of-sight velocities of galaxy systems, their radii and total luminosities [33], we decided to measure the $M_{1/2}$ masses of groups and clusters using the technique proposed by Wolf et al. [32] based on observational parameters of galaxy systems exclusively. Lyskova et al. [35] proposed very much the same method for estimating the masses of early-type galaxies (and galaxy clusters [34]) inside the radius $R_{\rm sweet}$, which is close to the effective radius $R_{\rm e}$. This method uses observational data: the surface brightness of stars or galaxies and the line-of-sight velocity dispersion.

To determine the effective radius $R_{\rm e}$ of a group or cluster of galaxies, we must first determine the total luminosity of the system. In our earlier papers [28–30] we determined the infrared luminosity of galaxy clusters. To this end, we used the results of the photometry of galaxies presented in the final version of 2MASS extended source catalog (XSC [36]). We extended the limiting magnitude of this catalog to $K_{\rm s} = 14\overset{\rm m}{.}7–15\overset{\rm m}{.}0$ using the dependence of the $(r-K)$ galaxy color on the SDSS $(u-r)$ color. We use a graphical method to determine the effective radius of a galaxy cluster containing half of the IR luminosity of the system. The main difference between our method and other similar techniques is that we consider the cumulative distribution of the number of galaxies (the profiles of galaxy systems) depending on the squared clustercentric radius. In our opinion, this is a simple and perhaps even a coarse but purely observation-based representation of the cluster profile. We could not substantiate this cluster representation theoretically. Figure 3 shows the cumulative distribution of the number of galaxies as a function of squared clustercentric distance for the Virgo (left) and A 2063 (right) clusters. We constructed such distributions for all the galaxy systems studied and found

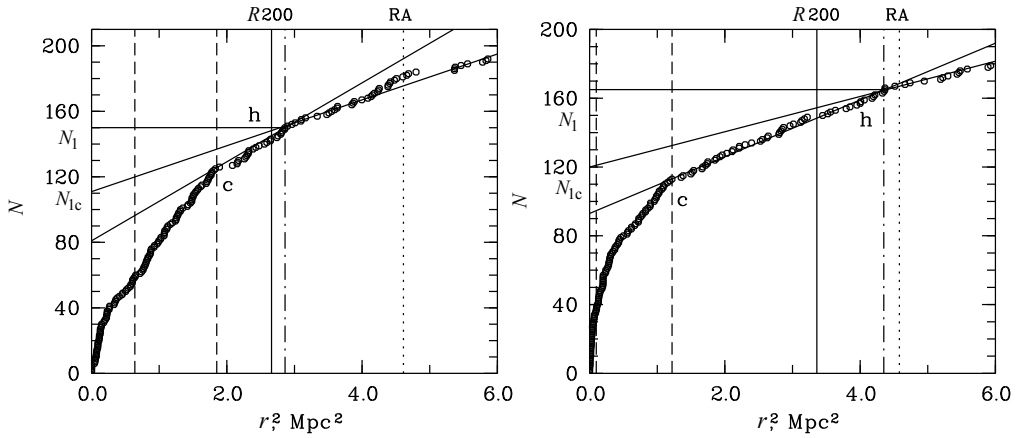

Fig. 3. Cumulative distribution of the number of galaxies as as a function of squared clustercentric distance for the Virgo (left) and A 2063 (right) clusters. The solid vertical line and the dotted line indicate the R_{200} and Abell R_A radii respectively. The dashed-and-dotted line indicates the $R_{\rm h}$ radius bounding the cluster: core (c) and halo (h); the dashed line indicates the $R_{\rm c}$ and $R_{\rm e}$ radii. Here N_1 and $N_{1\rm c}$ are the number of galaxies inside $R_{\rm h}$ before and after background subtraction respectively. The two solid lines show the distribution of galaxies located inside the halos of groups and clusters and the distribution of galaxies that do not belong to the halo.

empirically that the distributions for all clusters show a steep rise in the central part (the core) followed by linear increase of the number of galaxies located in the halo surrounding the cluster, and, finally, if the cluster is sufficiently isolated, by the linear increase of the number of galaxies located practically in the general field. The c and h letters in the figure indicate the radii of the cluster regions (core and halo) identified in this study.

Figure 4 shows the distributions for the remaining galaxy clusters. An analysis of the figures leads us to conclude that most of the galaxies in a cluster are located in its central region within the $R_{\rm h}$ radius. Our task is to identify this region (actually, identify the cluster), determine the number of galaxies with the contribution of background taken into account, compute their IR luminosity (also with the the background contribution subtracted), and estimate the effective radius of the cluster. As is evident from Fig. 3, inside the $R_{\rm h}$ radius there are N_1 galaxies including field objects and N_{1c} galaxies with field objects excluded. We use a graphical method to determine the number of cluster galaxies without field objects based on the slope of the distribution of galaxies outside the cluster halo. Here N_1 and N_{1c} are related by equation $N_{1c} = N_1 - \pi R_{\rm h}^2 \Sigma^N$, where the number density of galaxies (inside the $R_{\rm h}$ radius) is equal to $\Sigma^N = (N_1 - N_{1c})/(\pi R_{\rm h}^2)$. We determined the IR luminosity for the resulting galaxies, $L_{1c} = L_1/N_1 N_{1c}$, and found the effective radius containing half of the cluster luminosity. Note that this method does not work for the galaxy groups AWM 04 and A 1177 (of the "fossil group" type), each of which has a very bright galaxy at its center. In these cases when determining the effective radius we subtracted the luminosity of the brightest galaxy from the total luminosity of the group. No problems arise if we determine this radius using the technique described above as the radius containing half of the galaxies. A practically linear relation is known to exist between the number of galaxies inside the R_{200} radius and their IR luminosity [37].

Table 2 lists the parameters of galaxy groups and clusters (similar to those listed in Table 1) for the the region inside the effective radius $R_{\rm e}$ containing half of the L_K luminosity: the heliocentric redshift; number of galaxies with measured redshifts ($r_{\rm pet} < 17\overset{\rm m}{.}77$); core and halo radii, $R_{\rm c}$ and $R_{\rm h}$; the computed $R_{\rm e1}$ radius containing $L_K/2$; the computed $R_{\rm e2}$ radius containing $N/2$ galaxies; the dispersion of line-of-sight velocities $\sigma_{\rm c}$ with cosmological correction $(1+z)^{-1}$ applied; the $M_{1/2}$ mass, and $L_{K,1/2}$ IR luminosity (for $K \le 15^{\rm m}$). The luminosities of galaxies are determined in projection, in cylinders.

2.3. Measurement of the $M_{X,200}$ Mass

The baryonic component in galaxy clusters is mostly contained in the form of hot plasma whose mass distribution within virialized regions can be studied by analyzing the x-ray emission. This observed emission, combined with analytical models, can be used to reconstruct the distribution of gas density and gas temperature profile along the cluster radius. The resulting data are used to estimate the

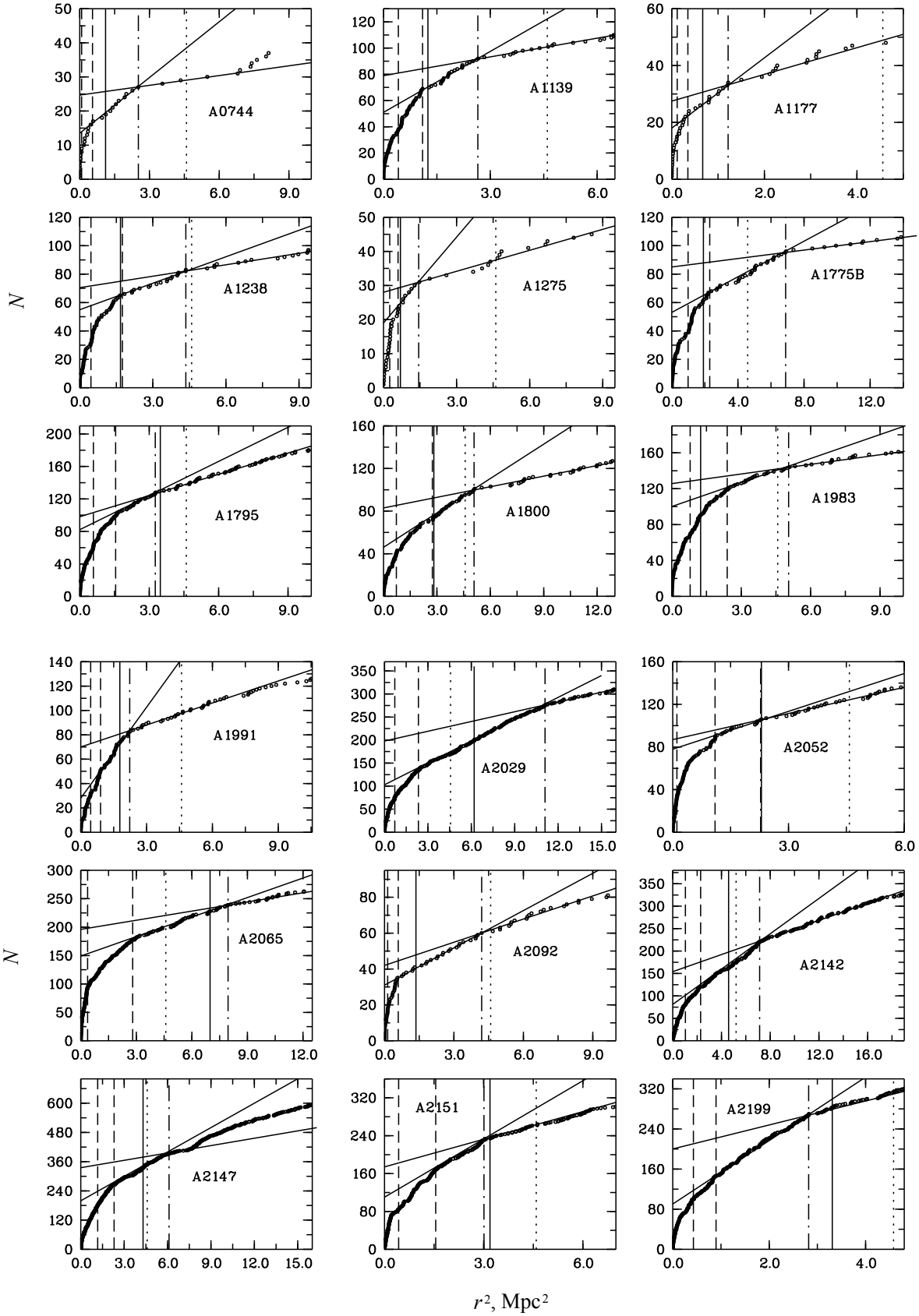

Fig. 4. Cumulative distribution of the number of galaxies as a function of squared distance to the center of the cluster or a group.

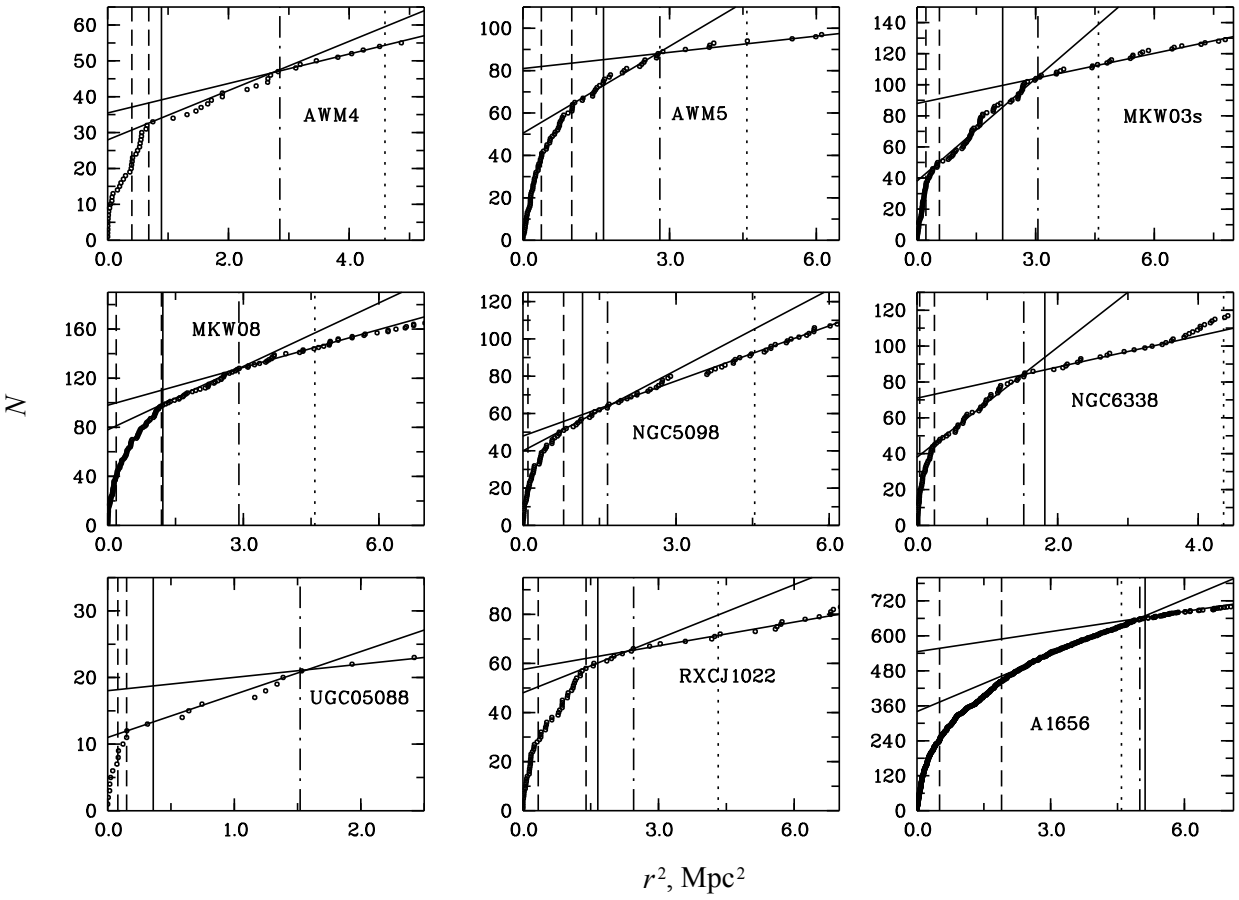

Fig. 4. (Contd.)

cluster mass within the r radius using hydrostatic equilibrium equations [6]:

$$M(<r) = -3.68 \times 10^{13} M_\odot\, T(r)\, r \times \left(\frac{d\log \rho_{\rm g}}{d\log r} + \frac{d\log T}{d\log r} \right), \quad (1)$$

where T and $\rho_{\rm g}$ are the gas temperature and density, respectively.

We adopted the published values for the masses of the groups and clusters computed in this way, which mostly refer to the region inside the R_{500} radius, and converted them to the masses inside the R_{200} radius ($M_{200} = 1.4\, M_{500}$). We list these masses in Table 1 along with the corresponding references. The table also lists the errors of the mean values in the cases where we found several measurements for the same group or cluster.

3. COMPARISON OF MASSES OF GALAXY GROUPS AND CLUSTERS DETERMINED USING DIFFERENT METHODS

We found that the mass of the virialized region of a galaxy cluster contained inside the R_{200} radius and determined from the dispersion of line-of-sight velocities of galaxies is approximately equal to 1.65 times the mass contained inside the effective radius. This dependence has the form

$$\log M_{200} = 1.05(\pm 0.01) \log(1.65\, M_{1/2}). \\ -0.71(\pm 0.19)$$

and is shown in Fig. 5. The dependence is derived by averaging the direct and inverse regression relations with the independent variables swapped. The standard deviation σ of the relation is equal to 0.17. The dashed-and-dotted lines in the figure show the 2σ deviations from the mean (dashed) line. The coefficient 1.65 is chosen so as to make the average difference of the masses $\log M_{200}$ and $\log(1.65\, M_{1/2})$ of galaxy clusters close to its minimum value. We found for our sample $\log M_{200} - \log(1.65\, M_{1/2}) = 0.02 \pm 0.03$.

The mass of the stellar population in galaxy clusters can be best traced by their IR luminosity and therefore we show in Fig. 6 the regression relations derived in the same way as those shown in Fig. 5 between the mass inside the R_{200} radius measured

from one-dimensional dispersion of line-of-sight velocities (left) and from the gas emission inside the x-ray region (right) on the one hand and the IR luminosity of galaxy clusters determined with the condition $M_K < -21^{\rm m}$ on the other hand. Note that we computed the corresponding R_{200}, N_{200}, and IR luminosity (we list it in Table 1) for $M_{X,200}$. The regression relations have the form:

$$\log M_{200} = 1.19(\pm0.01)\log L_K - 0.64(\pm0.15),$$

$$\log M_{X,200} = 1.23(\pm0.02)\log L_K - 1.25(\pm0.24).$$

The standard deviations of these relations are equal to 0.13 and 0.22, respectively. As is evident from the figure, the greater scatter (by a factor of 1.2) of the $\log M_{X,200}$–$\log L_K$ relation is due mostly to the deviations of $\log M_{X,200}$ (masses) of clusters A 2151 and NGC 5098, because their IR luminosities are estimated rather accurately, and to the deviation of the AWM 4 group ("fossil group"), where the luminosity of the giant cD galaxy is apparently underestimated. The resulting scatter of the $\log M_{200}$–$\log L_K$ relation (on the average amounting to 30%) allows the masses of galaxy systems to be estimated to a first approximation. The estimates are made assuming that deviations from the relation are mostly due to the uncertainty of the dynamic state of the systems (e.g., [3]), which affects the accuracy of the mass estimates. Furthermore, the dispersion of line-of-sight velocities of clusters may increase with decreasing galaxy luminosity or if there are many galaxies with emission lines. As Ramella et al. [3] pointed out, the total luminosity of the cluster can also be underestimated: e.g., because of the underestimated luminosity of cD galaxies or intergalactic stars. We found that for our sample the dispersion of line-of-sight velocities of galaxies does not increase with decreasing luminosity of galaxies.

Earlier a correlation has been found between the infrared luminosity of 93 galaxy clusters (actually between the stellar mass of the galaxies) measured from their K-band luminosity and the total hydrostatic mass with a scatter of about 32% [38]. Kravtsov et al. [39] calibrated this relation for 21 galaxy clusters and found a relation between the total stellar mass based on SDSS photometry and the total hydrostatic mass of cluster halos with a similarly steep slope of about 0.6 ± 0.1 and a scatter of about 29%. Andreon [40] determined the stellar masses of early-type galaxies in clusters from their optical fluxes (SDSS data) and found the resulting masses to agree well with hydrostatic masses with a small scatter. He also pointed out the possibility of estimating the stellar masses of clusters using IR data of future surveys.

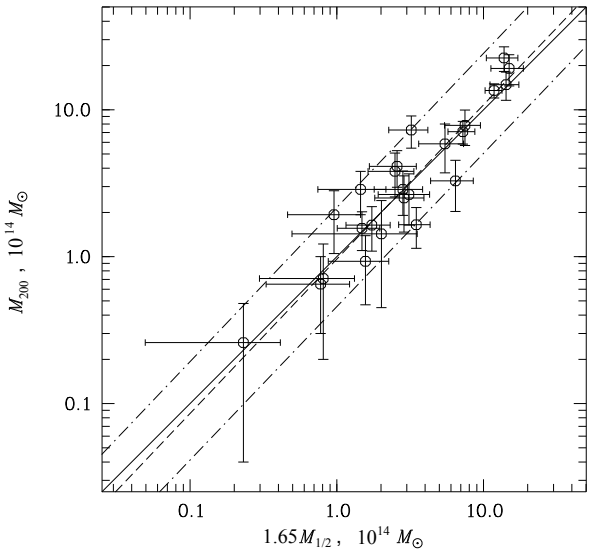

Fig. 5. Comparison of the masses of galaxy groups and clusters located inside R_{200} with the mass contained inside the effective radius $R_{\rm e}$. The solid line corresponds to the linear relation. The dashed line shows the regression relation ($M_{200} \propto 1.65\,M_{1/2}^{1.05\pm0.01}$). The dash-dotted lines show the 2σ deviations. The errors of masses correspond to the errors of measured line-of-sight velocity dispersions of galaxy systems.

For some galaxy systems no mass errors are shown in Fig. 6, because only one published measurement could be found. This means that the errors of estimated masses in the right-hand figure depend on the number of measurements, and those in the left-hand figure, on the error of the measured dispersion of line-of-sight velocities. An analysis of the figures leads us to conclude that both relations have practically the same slope within the quoted errors, although they have different scatter.

We compare the inferred masses in Fig. 7: $M_{X,200}$ vs. M_{200} (the left panel) and $M_{X,200}$ vs. $1.65\,M_{1/2}$ (the right panel). The regression relations have the form:

$$\log M_{X,200} = 1.01(\pm0.02)\log M_{200} - 0.39(\pm0.30),$$

$$\log M_{X,200} = 1.06(\pm0.02)\log(1.65\,M_{1/2}) - 1.10(\pm0.31).$$

Most of the galaxies are aligned along the line (the solid line in the left-hand figure) that presents the linear relation between the masses. The average differences of the masses are equal to:

$$\log M_{X,200} - \log M_{200} = -0.18 \pm 0.05,$$

$$\log M_{X,200} - \log(1.65\,M_{1/2}) = -0.17 \pm 0.05.$$

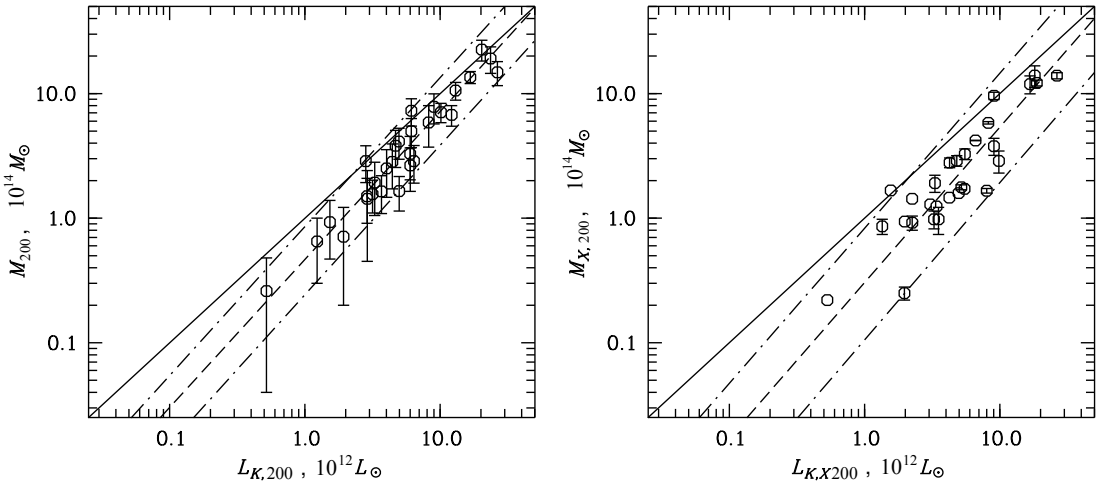

Fig. 6. Dependence of the mass M_{200} of galaxy groups and clusters measured from the dispersion of line-of-sight velocities of galaxies (left) and from x-ray emission of gas (right) on the K-band luminosities $L_{K,200}$ and $L_{K,X200}$ determined from galaxies brighter than $M_K = -21^{\rm m}$ located inside the corresponding virialized radii R_{200} listed in Table 1. The solid line corresponds to the linear relation. The dashed line shows the regression relations ($M_{200} \propto L_K^{1.19\pm0.01}$ in the left panel and $M_{200} \propto L_K^{1.23\pm0.02}$ in the right). The dash-dotted lines show the 2σ deviations. The mass errors in the left panel correspond to the errors of the measured dispersion of line-of-sight velocities of galaxy systems, and those in the right panel—to the errors of the mean.

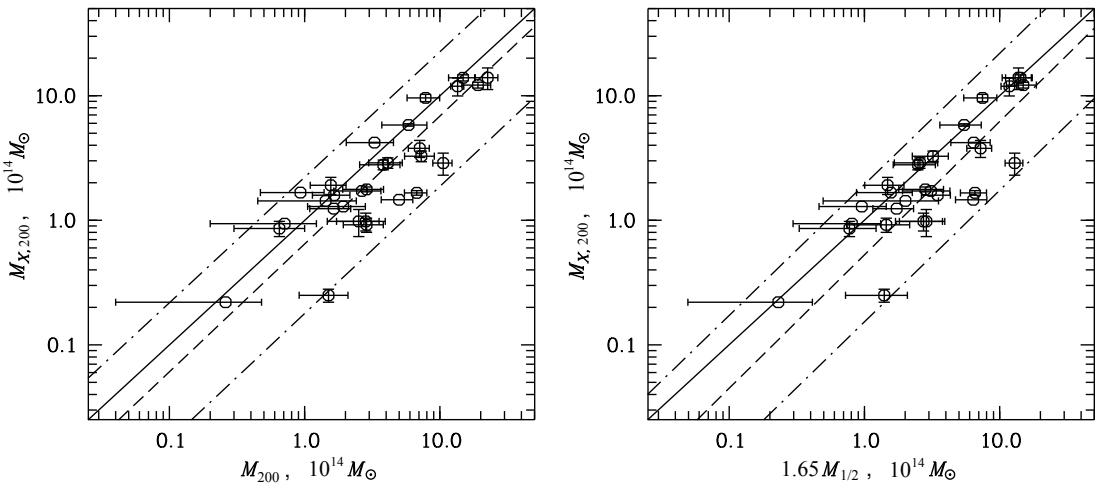

Fig. 7. Dependence of the mass of galaxy groups and clusters $M_{X,200}$ measured from x-ray gas emission on the mass measured from the dispersion of line-of-sight velocities of galaxies (left: within R_{200}; right: within $R_{\rm e}$). The solid line corresponds to the linear relation. The dashed line shows the regression relations ($M_{X,200} \propto M_{200}^{1.01\pm0.02}$ on the left and $M_{X,200} \propto 1.65\, M_{1/2}^{1.06\pm0.02}$ on the right). The dash-dotted lines show the 2σ deviations. The errors of the M_{200} and $1.65\, M_{1/2}$ masses correspond to the errors of measured dispersions of line-of-sight velocities of galaxy systems, the errors of the $M_{X,200}$ masses are the standard errors.

Table 2. Physical properties of galaxy groups and clusters inside $R_{\rm e}$

Cluster	$z_{\rm h}$	N_z	$R_{\rm c}$, Mpc	$R_{\rm h}$, Mpc	R_{e1}, Mpc	R_{e2}, Mpc	$\sigma_{\rm c}$, km s^{-1}	$M_{1/2}$, $10^{14}\,M_\odot$	$L_{K,1/2}$, $10^{12}\,L_\odot$
Virgo	0.003578	59	1.36	1.69	0.802	0.893	721 ± 94	3.87 ± 1.01	2.42
A 1656	0.023130	237	1.38	2.24	0.712	0.823	1040 ± 68	7.15 ± 0.94	7.19
MKW 08	0.026983	38	1.09	1.70	0.433	0.555	473 ± 77	0.90 ± 0.29	1.52
UGC 05088	0.027405	7	0.39	1.23	0.268	0.236	238 ± 90	0.14 ± 0.11	0.34
NGC 6338	0.029142	17	0.50	1.23	0.202	0.424	685 ± 166	0.88 ± 0.43	1.20
A 2199	0.030575	92	0.95	1.68	0.659	0.774	846 ± 88	4.38 ± 0.91	3.74
AWM 4	0.031980	20	0.82	1.69	0.629	0.490	404 ± 90	0.95 ± 0.42	0.49
A 1177	0.031944	12	0.59	1.10	0.344	0.327	385 ± 111	0.47 ± 0.27	0.42
A 2063	0.034457	45	1.10	2.09	0.378	0.418	746 ± 111	1.95 ± 0.58	2.46
A 2052	0.034908	32	1.05	1.52	0.336	0.427	708 ± 125	1.56 ± 0.55	2.05
AWM 5	0.035077	29	1.00	1.67	0.619	0.641	550 ± 102	1.74 ± 0.64	2.30
A 2147	0.036478	177	1.52	2.47	1.083	0.994	882 ± 66	7.83 ± 1.17	6.36
A 2151	0.035213	84	1.24	1.73	0.658	0.760	807 ± 88	3.98 ± 0.87	4.59
NGC 5098	0.037062	17	0.89	1.29	0.320	0.414	536 ± 130	0.85 ± 0.41	1.17
A 1139	0.039205	35	1.05	1.63	0.652	0.712	417 ± 70	1.05 ± 0.35	1.99
A 1983	0.044728	68	1.55	2.25	0.896	0.801	503 ± 61	2.11 ± 0.51	3.65
MKW 03s	0.045183	34	0.75	1.75	0.483	0.699	580 ± 99	1.51 ± 0.52	2.14
RXCJ 1022	0.054314	28	1.18	1.56	0.579	0.629	555 ± 105	1.66 ± 0.63	1.96
A 1991	0.059361	32	0.95	1.49	0.672	0.853	524 ± 93	1.75 ± 0.62	2.74
A 1795	0.062651	53	1.24	1.80	0.766	0.736	798 ± 110	4.53 ± 1.24	3.14
A 1275	0.062604	10	0.77	1.20	0.512	0.522	320 ± 101	0.49 ± 0.31	0.90
A 2092	0.066750	15	0.77	2.05	0.375	0.524	410 ± 106	0.58 ± 0.30	1.49
A 2065	0.073644	68	1.67	2.82	0.605	0.581	1220 ± 148	8.36 ± 2.03	7.40
A 0744	0.072600	7	0.74	1.59	0.279	0.546	685 ± 259	1.22 ± 0.92	1.03
A 1238	0.073740	27	1.29	2.08	0.680	0.674	545 ± 105	1.88 ± 0.72	2.84
A 1775B	0.075014	38	1.52	2.62	0.998	1.047	649 ± 105	3.90 ± 1.26	3.27
A 1800	0.075618	35	1.38	2.25	0.857	1.001	645 ± 109	3.31 ± 1.12	3.87
A 2029	0.077574	64	1.53	3.33	0.849	1.350	1072 ± 134	9.06 ± 2.26	9.13
A 2142	0.090113	81	1.52	2.67	1.025	1.107	952 ± 106	8.63 ± 1.92	8.08

The mass difference for eight galaxy systems—A 2063, AWM 5, NGC 5098, A 2147, A 2151, NGC 6338, RXCJ 1022, Virgo—is significant and deviations from the mean relation amount to 2σ (the dashed-and-dotted lines in the figures). If we reject these objects then the dynamic and hydrostatic masses of the remaining 21 groups and clusters of galaxies agree with each other to within 12%, i.e.,

$$\log M_{X,200} - \log M_{200} = -0.05 \pm 0.03,$$

$$\log M_{X,200} - \log(1.65\, M_{1/2}) = -0.05 \pm 0.03.$$

The median error of the determination of the M_{200} mass is equal to 30%. Seven outlier galaxy clusters are located in the region of Hercules supercluster. It is important that superclusters as regions of high number density of galaxies affect the properties of galaxy groups and clusters located inside them [41], and the differences between superclusters, i.e., actually the differences between the parameters of clusters and groups located inside them, may be due to their different evolutionary histories [42]. For example, we found that the relation between the L_K luminosity and the M_{200} mass for galaxy groups and clusters in the region of the rich Hercules supercluster is steeper than the corresponding relation in the region of the rich Leo supercluster located in the same redshift interval [30].

4. COMMENTS ABOUT SOME CLUSTERS AND GROUPS

An analysis of the data for discrepant galaxy clusters shows that these systems exhibit various signs of dynamic activity. The x-ray emission of gas in *Virgo* cluster shows, according to Böhringer et al. [43], that a large part of the cluster mass is centered on the galaxy M 87, with smaller concentrations around M 86 and M 49. It is also suggested that the galaxy M 86 is a part of a small group, which has merged with the main group. The mass of the cluster determined from the x-ray emission of gas is smaller than the mass determined from the dispersion of line-of-sight velocities of individual galaxies. Figure 1 (the bottom right panel) shows the velocity distribution of galaxies located inside the R_{200} radius, and the solid line shows the corresponding Gaussian. The dashed line shows the Gaussian for galaxies located in the central part of the distribution (centered on the galaxy M 87). The mass of the cluster determined from these galaxies agrees with the hydrostatic mass.

As for the group *NGC 5098* [44], optical data, x-ray emission, and simulations (made in terms of the two-body problem) show that this region contains two independent and gravitationally unbound groups. According to the above authors, the x-ray luminosity associated with the main group is insufficient for the groups to interact: the minimum mass bounding these groups should be at least a factor of 3–5 greater. According to the data of the above authors, there is a void in the velocity distribution of galaxies between the groups. SDSS data (Fig. 2, the bottom right panel) do not show this void, i.e., group members are intermixed, although one of the groups shows a well-defined peak in the distribution. We determined the overall velocity dispersion, mass, and IR luminosity. Note that the luminosity agrees with the mass inferred from σ and with the mass computed from the $\log M_{200}$–$\log L_K$ relation. We used the published hydrostatic mass (column 8 in Table 1) to compute σ, R_{200}, and determine the L_K luminosity (column 9 in Table 1). The mass computed from this luminosity by the $\log M_{X,200} - \log L_K$ relation is about three times the hydrostatic mass. Thus in our opinion our measured M_{200} mass should be preferred and can be considered as the upper limit for the mass of the system. Figure 2 (the bottom right panel) shows the histogram of line-of-sight velocities of galaxies located within R_{200}. The solid line shows the Gaussian corresponding to this distribution and the dashed line, the Gaussian for the galaxies (including the brightest one) that form the peak. The mass of the group inferred from the dispersion of line-of-sight velocities of these galaxies is equal to the hydrostatic mass.

In the *A 2151* cluster gas emission shows up in two galaxy groups (see, e.g., [45]), which are located within our inferred R_{200} radius. The group containing the brightest galaxy of the cluster is not located at the center but off the bulk of the galaxies. We therefore set the cluster center to coincide with the centroid of the distribution of galaxies. In addition, the brightest galaxy of the cluster has a peculiar velocity of -375 km s^{-1} relative to the average line-of-sight velocity of the system. In the *A 2147* cluster (Hercules supercluster), which is located in close vicinity to A 2151, the brightest galaxy is located at the cluster center and at the center of x-ray emission. However, the distribution of x-ray emission has a complex structure typical of the ongoing merger of the groups (e.g., [46]), which can be seen within the projected distance R_{200}. We subtracted the neighboring cluster A 2152 from A 2147. The rich clusters A 2147 and A 2151 are located close to each other and possibly exert mutual gravitational influence.

Galaxy clusters at the present epoch are dynamically active and grow by cannibalizing other galaxy groups and clusters. Different stages of the growth of such systems may have different effect on the measured dispersions of line-of-sight velocities of galaxies and the luminosity of the x-ray gas inside them. For example, simulations of the effects of the dynamic

state of galaxy clusters (mergers with other groups) on the measured hydrostatic masses performed by Nelson et al. [47] (see also references therein) showed that the masses determined assuming hydrostatic equilibrium may be underestimated. The above authors showed that the best epoch for measuring the masses of clusters is four billion years after the merger with another cluster.

5. MAIN CONCLUSIONS

When measuring the masses of collapsing objects (groups and clusters) without distinct boundaries one has to make assumptions concerning the sizes of these objects. Several methods for estimating the sizes of galaxy systems have been proposed in published studies. Currently the most commonly used method consists in selecting the cluster neighborhood of radius R_{200} such that within it the density exceeds 200 times the critical density of the Universe [13]. In this paper we report the results of our measurement of the dynamical masses for a sample of galaxy groups and clusters within two radii (R_{200} and $R_{\rm e}$) and their comparison with the masses inferred from the emission of hot gas filling their interiors. We determined the dynamic masses of galaxy clusters with a median error of 30%, which depends on the errors of the measured dispersion of line-of-sight velocities. Our inferred mass estimates are most likely the upper limits for the masses of the galaxy systems studied.

Our sample has the following parameters: redshifts $0.003 < z < 0.090$, masses $0.3{-}22.5 \times 10^{14}\ M_\odot$, and IR luminosities $0.5{-}26.5 \times 10^{12}\ L_\odot$. We determined the dynamic masses (M_{200} and $M_{1/2}$) of the galaxy systems considered for regions of radius R_{200} and of effective radius $R_{\rm e}$ containing half of the IR luminosity of the galaxy clusters studied. In this study we used a simple (observational) method for identifying galaxy groups and clusters and determination of their effective radii $R_{\rm e}$ from the observed cumulative distribution of the number of galaxies depending on squared clustercentric distance (Fig. 3, Section 2.2). We have not found theoretical justification for such a profile of galaxy systems.

To measure M_{200} and $M_{1/2}$, we used as the center the brightest galaxy in the cluster, which is usually located near the x-ray emission center, and considered galaxies with velocities deviating by more than 2.7σ as field objects. The masses of galaxy systems ($M_{X,200}$) determined from gas emission (published data) are measured for the region of radius R_{200} or converted from $M_{X,500}$. We obtained the following results.

(1) We developed an empirical method for identifying galaxy groups or clusters from the observed cumulative distribution of the number of galaxies depending on squared clustercentric distance. We also determined such parameters of galaxy systems as the dispersion of line-of-sight velocities, IR luminosity, and the number of galaxies at the effective radius.

(2) We show that the dynamic masses of galaxy groups and clusters for regions of radii R_{200} and $R_{\rm e}$ are related as $M_{200} \sim 1.65\, M_{1/2}$. We obtained the same relation between hydrostatic and dynamic masses for 21 clusters of the sample: $M_{X,200} \sim 1.65\, M_{1/2}$.

(3) The inferred dynamic (M_{200} and $1.65\, M_{1/2}$) and hydrostatic ($M_{X,200}$) masses for 21 groups and clusters of galaxies agree with each other to within 12%. The two masses for the remaining eight systems of galaxies, mostly those from the Hercules supercluster, deviate significantly from this relation.

Galaxy clusters are young systems that grow permanently by merging nearby groups, galaxies, and clusters. Their individual study using various methods may be of crucial importance from the point of view of their inclusion into samples used for the determination of cosmological parameters.

ACKNOWLEDGMENTS

This research has made use of the NASA/IPAC Extragalactic Database (NED, `http://nedwww.ipac.caltech.edu`), Sloan Digital Sky Survey (SDSS, `http://www.sdss.org`), and Two Micron All Sky Survey (2MASS, `http://www.ipac.caltech.edu/2mass/releases/allsky/`).

REFERENCES

1. A. A. Vikhlinin, A. V. Kravtsov, M. L. Markevich, et al., Uspekhi Fiz. Nauk **184**, 349 (2014).
2. M. Girardi, G. Giuricin, F. Mardirossian, et al., Astrophys. J. **505**, 74 (1998).
3. M. Ramella, W. Boschin, M. Geller, et al., Astron. J. **128**, 2022 (2004).
4. A. Muzzin, H. K. C. Yee, P. B. Hall, and H. Lin, Astrophys. J. **663**, 150 (2007).
5. A. J. R. Sanderson, T. J. Ponman, A. Finoguenov, et al., Monthly Notices Royal Astron. Soc. **340**, 989 (2003).
6. A. Vikhlinin, A. Kravtsov, W. Forman, et al., Astrophys. J. **640**, 691 (2006).
7. Y. Chen, T. H. Reiprich, H. Böhringer, et al., Astron. and Astrophys. **466**, 805 (2007).
8. N. Okabe, M. Takada, K. Umetsu, et al., Publ. Astron. Soc. Japan **62**, 811 (2010).
9. A. Diaferio and M. J. Geller, Astrophys. J. **481**, 633 (1997).

10. I. D. Karachentsev and O. G. Nasonova, Monthly Notices Royal Astron. Soc. **405**, 1075 (2010).
11. P.Nurmi, P. Heinämäki, T. Sepp, et al., Monthly Notices Royal Astron. Soc. **436**, 380 (2013).
12. K. N. Abazajian, J. K. Adelman-McCarthy, M. A. Aqüeros, et al., Astrophys. J. Suppl. **182**, 543 (2009).
13. R. G. Carlberg, H. K. C. Yee, E. Ellingson, et al., Astrophys. J. **485**, L13 (1997).
14. K. Rines and A. Diaferio, Astron. J. **132**, 1275 (2006).
15. G. A. Mamon, A. Biviano, and G. Murante, Astron. and Astrophys. **520**, A30 (2010).
16. A. Biviano, G. Murante, S. Borgani, et al., Astron. and Astrophys. **456**, 23 (2006).
17. T. H. Reiprich and H. Böhringer, Astrophys. J. **567**, 716 (2002).
18. H. J. Eckmiller, D. S. Hudson, and T. H. Reiprich, Astron. and Astrophys. **535**, A105 (2011).
19. M. Sun, G. M. Voit, M. Donahue, et al., Astrophys. J. **693**, 1142 (2009).
20. A. Finoguenov, T. H. Reiprich, and H. Böhringer, Astron. and Astrophys. **368**, 749 (2001).
21. R. Piffaretti, Ph. Jetzer, J. S. Kaastra, and T. Tamura, Astron. and Astrophys. **433**, 101 (2005).
22. F. Gastaldello, D. A. Buote, P. J. Humphrey, et al., Astrophys. J. **669**, 158 (2007).
23. E. Pointecouteau, M. Arnaud, and G. M. Pratt, Astron. and Astrophys. **435**, 1 (2005).
24. A. I. Kopylov and F. G. Kopylova, Astrophysical Bulletin **62**, 311 (2007).
25. A. I. Kopylov and F. G. Kopylova, Astrophysical Bulletin **64**, 207 (2009).
26. A. I. Kopylov and F. G. Kopylova, Astrophysical Bulletin **65**, 205 (2010).
27. A. I. Kopylov and F. G. Kopylova, Astrophysical Bulletin **67**, 17 (2012).
28. F. G. Kopylova and A. I. Kopylov, Astrophysical Bulletin **64**, 1 (2009).
29. F. G. Kopylova and A. I. Kopylov, Astronomy Letters **37**, 219 (2011).
30. F. G. Kopylova and A. I. Kopylov, Astronomy Letters **39**, 1 (2013).
31. E. J. Tollerud, J. S. Bullock, G. J. Graves, and J. Wolf, Astrophys. J. **726**, 108 (2011).
32. J. Wolf, G. D. Martinez, J. S. Bullock, et al., Monthly Notices Royal Astron. Soc. **406**, 1220 (2010).
33. R. Schaffer, S. Maurogordato, A. Cappi, and F. Bernardeau, Monthly Notices Royal Astron. Soc. **263**, L21 (1993).
34. N. Lyskova, Astronomische Nachrichten **334**, 360 (2013).
35. N. Lyskova, E. Churazov, A. Moiseev, et al., Monthly Notices Royal Astron. Soc. **441**, 2013 (2014).
36. T. H. Jarrett, T. Chester, R. Cutri, et al., Astrophys. J. **119**, 2498 (2000).
37. K. Rines, M. J. Geller, A. Diaferio, et al., Astron. J. **128**, 1078 (2004).
38. Y.-T. Lin, J. J. Mohr, and S. A. Stanford, Astrophys. J. **610**, 745 (2004).
39. A. Kravtsov, A. Vikhlinin, and A. Meshscheryakov, submitted to Astrophys. J. ; arXiv:1401.7329.
40. S. Andreon, Astron. and Astrophys. **548**, A83 (2012).
41. M. Einasto, E. Saar, V. J. Maártinez, et al., Astrophys. J. **685**, 83 (2008).
42. M. Einasto, L. J. Liivamägi, E. Tempel, et al., Astron. and Astrophys. **542**, A36 (2012).
43. H. Böhringer, U. G. Briel, R. A. Schwartz, et al., Nature **368**, 828 (1994).
44. A. Mahdavi, A. Finoguenov, H. Böhringer, et al., Astrophys. J. **622**, 187 (2005).
45. Z. Huang and G. L. Sarazin, Astron. and Astrophys. **461**, 622 (1996).
46. W. Forman, Chandra proposal ID #03800400 (2001).
47. K. Nelson, D. H. Rudd, L. Shaw, and D. Nagai, Astrophys. J. **751**, 121 (2012).

Translated by A. Dambis